Kinetic Analysis of Copper(I)/Feringa-Phosphoramidite Catalyzed AlEt₃ 1,4-Addition to Cyclohex-2-en-1-one

Darren Willcox,[†] Ryan Nouch,[†] Alexander Kingsbury,[†] David Robinson,[‡] Joe V. Carey,[§] Steve Brough,[§] and Simon Woodward*,[†]

[†]GSK Carbon Neutral Laboratories for Sustainable Chemistry, University of Nottingham, Jubilee Campus, Nottingham NG7 2TU, United Kingdom

[‡]Department of Chemistry and Forensics, School of Science and Technology, Nottingham Trent University, Clifton Lane, Nottingham NG11 8NS, United Kingdom

[§]Key Organics Ltd, Highfield Road Industrial Estate, Camelford, Cornwall PL32 9RA, United Kingdom

S *Supporting Information*

ABSTRACT: ReactIR studies of mixtures of AlEt₃ (**A**) and cyclohex-2-en-1-one (**CX**) in Et₂O indicate immediate formation of the Lewis acid−base complex **CX·A** at −40 °C ($K = 12.0$ M^{-1}, $\Delta G°_{react} = -1.1$ kcal mol^{-1}). Copper(I) catalysts, derived from precatalytic Cu(OAc)₂ (up to 5 mol %) and (*R,S,S*)-P(binaphtholate){N(CHMePh)₂} (Feringa's ligand (**L**), up to 5 mol %) convert **CX·A** (0.04−0.3 M) into its 1,4-addition product enolate (**E**) within 2000 s at −40 °C. Kinetic studies (ReactIR and chiral GC) of **CX·A**, **CX**, and (*R*)-3-ethylcyclohexanone (**P**, the H$^+$ quenching product of enolate **E**) show that the true catalyst is formed in the first 300 s and this subsequently provides **P** in 82% ee. This true catalyst converts **CX·A** to **E** with the rate law [Cu]$^{1.5}$[L]$^{0.66}$[CX·A]^1 when [L]/[Cu] ≤ 3.5. Above this ligand ratio inhibition by added ligand with order [L]$^{-2.5}$ is observed. A rate-determining step (rds) of Cu₃L₂(**CX·A**)₂ stoichiometry is shown to be most consistent with the rate law. The presence of the enolate in the active catalyst best accounts for the reaction's induction period and molecularity as [**E**] ≡ [**CX·A**]. Catalysis proceeds through a "shuttling mechanism" between two C_2 symmetry related ground state intermediates. Each turnover consumes 1 equiv of **CX·A**, expels one molecule of **E**, and forms the new Cu−Et bond needed for the next cycle. The observed ligand (**L**) inhibition and a nonlinear ligand **L** ee effect on the ee of **P** are well simulated by the kinetic model. DFT studies (ωB97X-D/SRSC) support coordination of **CX·A** to the groundstate Cu trimer and its rapid conversion to **E**.

KEYWORDS: conjugate addition, mechanism, asymmetric, aluminum, copper, density functional theory
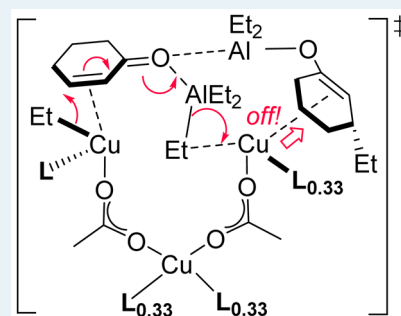
INTRODUCTION

Copper-catalyzed conjugate (1,4-)additions of alkyl organometallic reagents to Michael acceptors have become "go to" methods for enantioselective C−C bond construction, due to their reliability and often exceptional (frequently 90−95% ee) selectivities.[1] Typically, organozinc and Grignard reagents are employed as the terminal alkyl (R$^-$) source with a wide range of in situ formed copper(I) catalysts using diverse chiral ligands (**L**), including phosphines, N-heterocyclic carbenes (NHCs), and especially phosphoramidites.[2] The consensus mechanistic view of these 1,4-additions to enones (and related Michael acceptors), catalyzed by "RCuL$_n$", is given in Scheme 1.[3] Rapid reduction by MR (e.g., RMgX, ZnR₂) of copper(II) precatalysts means that only catalytic cycles starting from Cu^I operate. Initial π complexes **1**[4] are thought to undergo oxidative addition to σ-alkyl Cu^{III} complexes **2**.[5] The reductive elimination step is thought to be the stereodetermining turnover-limiting step, and this has been proposed to be strongly accelerated by coordination of π-acceptor ligands to the σ-Cu^{III} intermediate, providing enolates **3**.[1−3] The organocopper byproduct is then recycled to **1** to restart the catalytic cycle. The role of the bridging ligand (**X**) is to arrange the hard (**M**) and soft (Cu^I) Lewis acidic sites to provide dual activation for the Michael acceptor; both halides and pseudohalides have been used in this role. Hard evidence (as opposed to mechanistic conjecture) supporting the intimate details of the transition states providing such cycles is limited but has been described for Grignard additions (e.g., the structure of **4** has been deduced through kinetic and NMR studies of isolable model complexes of the reaction intermediates).[6] On the basis of kinetic studies transition state **5** was proposed for ACA reactions of ZnEt₂;[7] it is essentially a transposition of Noyori's proposal for 1,4-ZnEt₂ addition (from an earlier kinetic study of achiral sulfonamide catalysts[8]) but with an added chiral ligand. Through intensive NMR studies of CuX/**L** model systems (mostly in CD₂Cl₂) Gschwind[9] and co-workers proposed the hypothesis that the dominant transition state in "real" catalytic systems adding ZnEt₂ to cyclohex-2-en-1-one must be **6**.
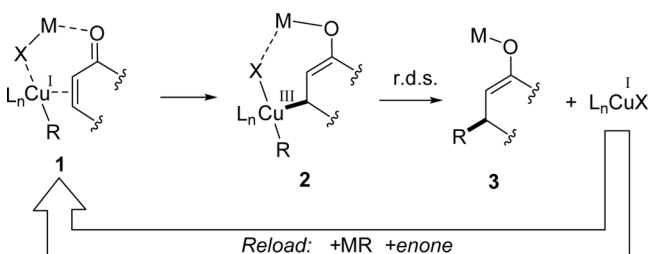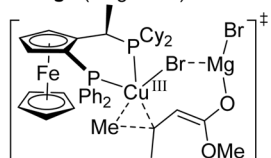
Scheme 1. Contemporary Understanding of the Mechanism of Catalytic Asymmetric Conjugate Addition (ACA) and a Summary of Evidence Cited to Support Such Proposals[a]
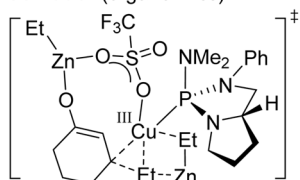

Feringa (Grignards):

4 *based on:*
- 2nd order consumption of a (Cu_2L_2) precursor
- Cu-Me detected in precursor complex
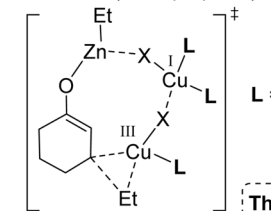- *Z/E* enone interconversion

Schrader (organozincs):

5 *based on:*
- Approximate first order kinetic dependance on [CuL]
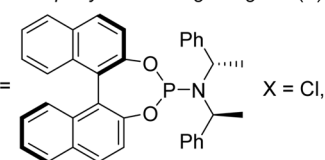- Approximate first order kinetic dependance on [ZnEt₂]

Gschwind (NMR proposal):

exemplary with Feringa's ligand (L)

L =

X = Cl, I

The same ligand (L) is used in our own paper for all kinetic studies

6 *based on:*
- DOSY NMR studies of precursors in CD_2Cl_2
- Cu-Et detected by magnetization transfer NMR studies

[a]Throughout this present paper (*R,S,S*)-Feringa's ligand (**L**) above has been used for all studies.

In the past decade the use of organoalanes (AlR_3) has become a popular modern variant for ACA reactions.[10] Very reactive catalytic systems are realized, allowing even for the formation of chiral quaternary centers by addition to β,β-disubstituted Michael acceptors.[1,11] Surprisingly, very little is known[12] about the critical transition state responsible for catalyst turnover in copper-promoted 1,4-additions of AlR_3 to enones, despite their common usage in the synthetic community.[10] Gschwind's proposal that speciation in ACA reactions is dominated by a single entity[9] suggests that classical reaction kinetics might be an effective way of estimating the composition of the $AlR_3/Cu^I/L$ active species (e.g., Cu_xL_y etc.) through reaction component order analysis. This prompted us to undertake a kinetic study of the model transformation of Scheme 2, based on a mixture of cyclohex-2-en-1-one (cyclohexenone, **CX**) and $AlEt_3$ (**A**) catalyzed by precatalytic $Cu(OAc)_2$ (**Cu**) in the presence of the optimal (*R,S,S*)-Feringa ligand (**L**, structure in Scheme 1). On workup the initially formed enolate (**E**) is converted to the enantioenriched ketone product (**P**).

Scheme 2. Model System Studied in This Publication: Cyclohex-2-en-1-one (CX), AlEt₃ (A), Cu(OAc)₂ (and Its Derived Copper(I) Reduction Product) (Cu), and (R,S,S)-Feringa Ligand (L), Leading to the Formation of the (R)-Enolate (E) and, on Its Hydrolysis, the (R)-Ketone Product (P)
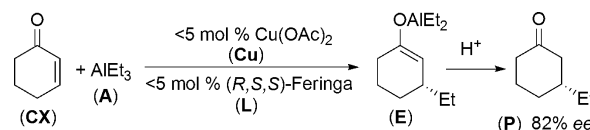

■ RESULTS

Formation of a CX·A Adduct. Mixing cyclohex-2-en-1-one (**CX**) and $AlEt_3$ (**A**) at −40 °C in Et_2O instantaneously gives a bright yellow solution that is stable for at least 30 min under these conditions. After aqueous quenching (2 M, aqueous HCl), **CX** is recovered quantitatively, indicating that no uncatalyzed 1,4-addition takes place under these conditions and that all other irreversible uncatalyzed processes are also negligible. The nature of the bright yellow reactive intermediate was investigated by ReactIR-monitored titration of **A** into **CX** (runs 1 and 2 in the Supporting Information). The intensity of the carbonyl stretching signal of **CX** (1676 cm⁻¹) falls after addition of each **A** aliquot as a new species with ν(C=O) 1630 cm⁻¹ grows in (Figure 1). Variation of the **CX**:**A** stoichiometry
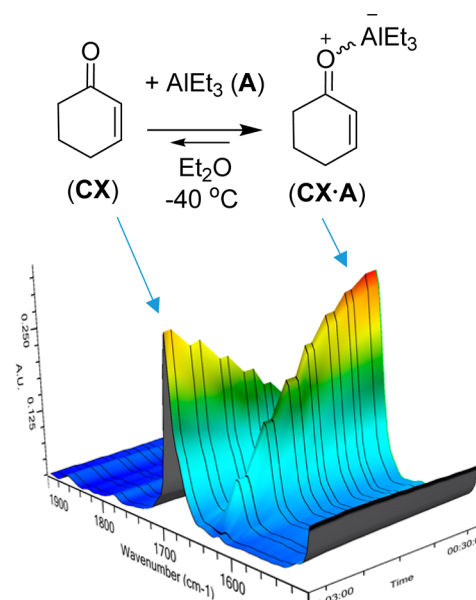
Figure 1. Formation of **CX·A** from **CX** and **A** (titrated in at ca. 0.1 equiv steps) in Et_2O at −40 °C. Complexation is complete within the time of mixing (<5 s) and provides $K = 12.0(8)$ M⁻¹. The values in parentheses indicate the standard deviation in the last digit based on linear correlations of $R^2 > 0.99$ for all fitted data.

indicates that the 1:1 Lewis acid−base complex **CX·A** is formed.[13,14] Fitting the appropriate reaction isotherm (runs 1 and 2 in the Supporting Information) gives the association constant $K = 12.0(8)$ M⁻¹ between **A** and **CX**, corresponding to a ΔG°_{react} value of −1.1 kcal mol⁻¹ at −40 °C. On the basis of the calculated **CX** and **CX·A** concentrations (between 129 and 481 mM and between 3 and 207 mM, respectively) the molar constants were determined as $\varepsilon_{CX} = 0.565$ M and $\varepsilon_{CX·A} = 0.697$ M. In order to attain accurate absolute quantification of
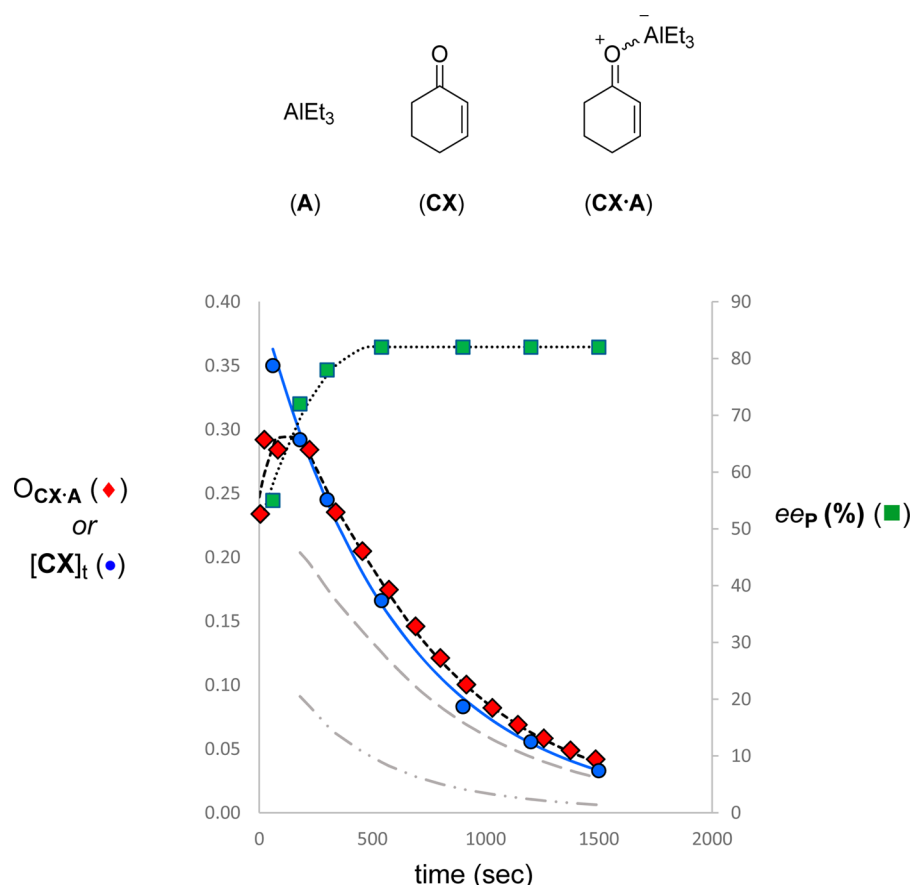
Figure 2. Representative monitoring of prereduced Cu(OAc)$_2$/L (1/1.5 mol %) catalyzed 1,4-addition of AlEt$_3$ (**A**, 0.35 M) to cyclohex-2-en-1-one (**CX**, 0.39 M) at −40 °C. The disappearance of **CX·A** was monitored via the intensity of its 1630 cm^{-1} IR stretch. Consumption of **CX** and the enantiomeric excess of the resultant product ee$_P$ were determined by Krause's cryogenic sampling method[17] via subsequent chiral GC assay (Lipodex A). Key: observed absorbance (O$_{CX·A}$) of **CX·A** (red ◆) via ReactIR; concentration **CX** (blue ●) and enantiomeric excess of product **P** (green ■) via chiral GC. The gray lines show calculated AlEt$_3$-bound cyclohex-2-en-1-one species [**CX·A**]$_{t,calc}$ (− −) and free cyclohex-2-en-1-one [**CX**]$_{t,calc}$ (−·−). The solid blue line (—) confirms the correlation [**CX$_{TOT}$**]$_t$ = free [**CX**]$_t$ + [**CX·A**]$_t$ detected in the GC experiments. For derivations see Figure S3 in the Supporting Information.

[**CX·A**], careful zero calibration of the ReactIR setup is required. The calculated $\Delta\Delta G$(−40 °C) difference between the related, experimentally determined, MeAl(BHT)$_2$(O=CPh$_2$) and MeAl(BHT)$_2$(OEt$_2$) (BHT = 2,6-di-*tert*-butyl-4-methyl-phenolate) using the data of Power[13] is similar at $\Delta G°_{react}$ = −1.45 kcal mol^{-1}.

Further credence to the proposal of Figure 1 is given by simple DFT modeling at the CAM-B3LYP/6-31G(d,p) level (Supporting Information). The calculated $\Delta G°_{react}$ values for exchange of Et$_3$Al·OEt$_2$ (the expected AlEt$_3$ speciation in Et$_2$O at −40 °C) with **CX** to provide the *syn* or *anti* isomers of **CX·A** are −6.4 and −6.1 kcal mol^{-1}, respectively. This is broadly in line with the experimentally observed free energy. These simple (gas-phase) calculations overestimate $\Delta G°_{react}$, as the effect of solvation is ignored. The presence of an Et$_2$O solvent cage around **CX·A** is expected to favor back-reaction to **A·OEt$_2$**. Similarly, the predicted ratio of the carbonyl stretching frequencies ν(C=O)$_{CX}$/ν(C=O)$_{CX·A}$ for *syn*-/*anti*-**CX·A** vs **CX** is calculated as ∼1.05 (CAM-B3LYP/6-31G(d,p)), in comparison to the experimental ratio of 1.03 (1676/1630 cm^{-1}).

Catalyst Order in CX·A. The reaction order of Scheme 2 in **CX·A** is formally attained from the slope of plots of ln k_{obs} as a function of ln[**CX·A**]$_0$ for the catalytic reaction at time t = 0. The adduct's initial concentration [**CX·A**]$_0$ can be calculated
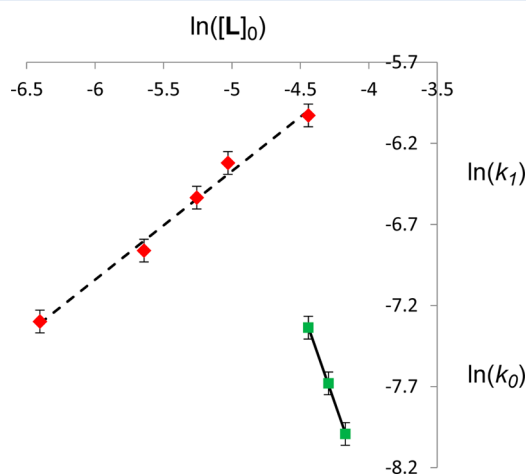
from the known added [**CX**]$_0$ and [**A**]$_0$ via K = 12.0(8) M^{-1} (eq 8 in the Supporting Information). Preliminary monitoring of a standard Cu(OAc)$_2$ (**Cu**) catalyzed (3.0 mM, 1 mol %) reaction using (R,S,S)-Feringa ligand (**L**) (4.5 mM, 1.5 mol %) with **CX** (0.35 M) and **A** (0.39 M, 1.2 equiv) reveal the presence of an induction period in the first ca. 200−300 s (Figure 2). This was most clearly demonstrated by the rise of product ee$_P$ as a function of time[17] and the maximum seen early on in the absorbance (O$_{CX·A}$) of species **CX·A**. The induction period is not associated with formation of Cu^I, as the Cu(OAc)$_2$/L mixture had already been cleanly reduced by prior treatment with AlEt$_3$ (125 equiv, 10 min, −40 °C)[15] prior to initiating the kinetic run by addition of **CX**. The homogeneous copper(I) precatalyst generated by prereduction is also stable under these conditions in this time frame.[16]

In the induction period (0−300 s) catalyst genesis and immediate subsequent catalytic cyclohex-2-en-1-one (**CX**) turnover compete; beyond it, catalysis is clearly dominated by a single copper species that provides the product (**P**) in ∼82% ee. Post induction, the disappearance of [**CX**] and [**CX·A**] both fit first-order behavior best (R^2 = 0.98−0.99+)[18] and correlation of the ReactIR and GC monitoring can be shown by their data interconversion (Figure 2 and Figure S3 in the Supporting Information) within experimental error. By fitting O$_{CX·A}$(1630 cm^{-1}) to [**CX·A**] beyond 300 s using [**CX·A**]$_0$ exp(−k_1t), the

induction period can thus be mathematically eliminated (runs 3−6 in the Supporting Information). In these trials the **Cu:L** ratio was kept fixed at 1:1.5 ($\pm$0.05) with nominal $[\mathbf{Cu}]_0 = 3.5$ and $[\mathbf{L}]_0 = 5$ mM and with $[\mathbf{CX \cdot A}]_0$ in the range 40−300 mM. The desired $\ln[\mathbf{CX \cdot A}]_0$ vs $\ln k_1$ plot provided a best-fit slope of 1.0 (Figure S4 in the Supporting Information) commensurate with the enantioselective catalytic reaction being first order in $\mathbf{CX \cdot A}$.[18] In practice, due to the presence of the induction period and experimental offsets in $O_{\mathbf{CX \cdot A}}$ it was easier to study change in $[\mathbf{CX \cdot A}]$, as this leads directly to k_1 (which is independent of the measured $[\mathbf{CX \cdot A}]_0$, avoiding tedious calibration of the crude absorbance (typically the value of $A_{\mathrm{obs},0}$ was ~0.35) and also avoiding repetitive checking of experimental offsets in absorbance).

Catalyst Order in Cu. Prereduction of $\mathrm{Cu(OAc)_2}$ with $\mathrm{AlEt_3}$ in the presence of **L** leads to quantitative formation of a stable $\mathrm{Cu^I}$ precatalyst with concentration $[\mathbf{Cu}]$.[16] By maintenance of a constant **Cu:L** ratio of 1:1.5 ($\pm$0.05) and variation of the $[\mathbf{Cu}]_0$ concentration in the range 1−6 mM at a constant $[\mathbf{CX \cdot A}]_0$ of 220 mM the order of the enantioselective reaction in copper(I) (**Cu**) could be determined. Reactions were monitored by ReactIR using post induction period decay data from $O_{\mathbf{CX \cdot A}}$ (runs 7−10 in the Supporting Information). Data from these trials were fitted to $[\mathbf{CX \cdot A}]_0 \exp(-k_1 t)$. A $\ln[\mathbf{CX \cdot A}]_0$ vs $\ln k_1$ plot provided a best-fit slope of 1.5 (Figure S5 in the Supporting Information) indicating that, post induction period, the enantioselective catalytic reaction is best described by a $[\mathbf{Cu}]^{1.5}$ order term.

Catalyst Order in L. At fixed copper concentration (3.5 mM) the rate of the catalytic reaction shows both ligand acceleration and ligand retardation regions. Initial $\ln[\mathbf{L}_0]$ vs $\ln k_1$, where the k_1 value was derived from the first-order decay of $O_{\mathbf{CX \cdot A}}$ for the species $\mathbf{CX \cdot A}$, gives a ligand acceleration order of 0.67 for regimes $0.5 \leq [\mathbf{L}]:[\mathbf{Cu}] \leq 3.5$ (Figure 3). For ligand concentrations where $[\mathbf{L}]:[\mathbf{Cu}] \geq 3.5$, a transition to zero-order kinetics is observed, providing an inhibition order of −2.5 in ligand (Figure 3 and Figures S6 and S7 in the Supporting Information). As these ligand orders provide critical pointers to

the **Cu:L** ratio in the transition state leading to asymmetric C−C bond formation, they were also determined by a GC study of $[\mathbf{CX}]_t$ (see the Supporting Information). The average of three separate analyses across both GC and ReactIR data gave ligand reaction orders of 0.66 and −2.52 for the separate ligand acceleration and retardation processes respectively (runs 9 and 11−23 in the Supporting Information). The only difference detected between the ReactIR and GC studies was that the greater data density of the former allowed the detection that the retardation process fits better to zero-order, rather than first-order, kinetics.

Data attained from the ReactIR kinetic studies of the dependence on **CX·A**, **Cu**, and **L** are collected together in Table 1.
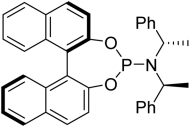
■ DISCUSSION

The presence of competing catalyst genesis followed by turnover in its early stages made the chemistry of Scheme 2 more suited to classical reaction order investigations rather than reaction progression analysis,[19] in our hands at least. Formation of the active catalyst for Scheme 2 is not associated with $\mathrm{Cu(OAc)_2}$ reduction, as a prereduction protocol is used prior to turnover initiation by **CX** addition. A similar catalyst induction period was also noted, but discounted, in Noyori's original rate studies of sulfonamide 1,4-addition catalysts—even though in this case no reduction is possible, as $\mathrm{Cu^I}$ sources were used from the outset.[8] The possibility that the enolate species **E**, formed in the initial induction period, might be involved in the formation of a more active and selective catalyst was also not considered at that time. Post induction period, our ligand-accelerated copper-catalyzed 1,4-addition of $\mathrm{AlEt_3}$ to cyclohex-2-en-1-one shows the rate law rate $\propto [\mathbf{CX \cdot A}]^1 [\mathbf{Cu}]^{1.5} [\mathbf{L}]^{0.66}$. One simple transition state stoichiometry deducible from this rate law is twice this: $\mathrm{Cu_3 L_{1+x} CX_2 A_2}$ ($x \approx 0.33$). This is not in line with behavior analogous to complexes **4−6** being involved as, in the simplest analysis, these would imply transition state stoichiometries of CuLCXA (Grignard), $\mathrm{CuLCXA_2}$ (organozinc), and $\mathrm{Cu_2 L_3 CXA}$ (NMR proposal), respectively. In their solution model studies[9] Gschwind and co-workers also detected an alternative to their dimeric $[\mathrm{L_2 Cu}(\mu\text{-Cl})_2 \mathrm{CuL}]$ precatalysts, which was the trigonal complex $[\mathrm{Cu}(\mu\text{-Cl})\mathrm{L}]_3$. This form is (depending on reaction conditions) nearly isoenergetic with the dimer and favored by lower **L:Cu** ratios and ethereal-based solvent systems. Structures based on $(\mathrm{CuL})_3$ were originally argued against, in favor of $\mathrm{Cu_2 L_3}$, on the basis that catalyst stereoselectivity in $\mathrm{ZnEt_2}$ 1,4-addition was maximized at $\mathbf{L:Cu} = 1.5$ for zinc-based additions.[9,20] This is not the case in the aluminum catalysis of Scheme 2, where the product ee remains high (82%) down to $\mathbf{L:Cu} = 0.45$, rather supporting a $\mathrm{Cu_3:L_{1.3}}$ ratio in events leading up to and including the rate-determining step.

Mechanistic Proposal. Any mechanistic proposal, for the asymmetric 1,4-$\mathrm{AlEt_3}$ addition catalyzed by $\mathrm{Cu^I/L}$ studied here, has to account for the presence of the observed induction period and the inhibition seen at high phosphoramidite **L** (relative to **Cu**) concentrations where rate $\propto [\mathbf{L}]^{-2.5}$. One hypothesis consistent with these requirements, and the observed reagent orders, is shown in Scheme 3. The transition state (**7**) allows rapid interconversion between two C_2 related equivalent intermediates (**8**). Each catalytic turnover ($\mathbf{8} \rightarrow \mathbf{7} \rightarrow C_2\text{-}\mathbf{8}$) results in clean interconversion of copper sites $\mathrm{Cu_A}$ and $\mathrm{Cu_B}$. In the early stages of the reaction, as no enolate (**E**) is available, the concentration of **7** is limited and an induction

Figure 3. ReactIR ligand (**L**) order plot for catalysis of Scheme 2 showing both acceleration (rate $\propto [\mathbf{L}]^{0.67(4)}$) and deceleration (rate $\propto [\mathbf{L}]^{-2.42(5)}$) regions for $[\mathbf{Cu}] = 3.5$ mM (1 mol %). The values in parentheses indicate the standard deviation in the last digit on the basis of linear correlations of $R^2 > 0.99$ for all fitted data (red ◆, k_1, first order for ligand acceleration; green ■, k_0, zero order for ligand deceleration).

Table 1. Summary of the ReactIR Investigations Carried out in This Study

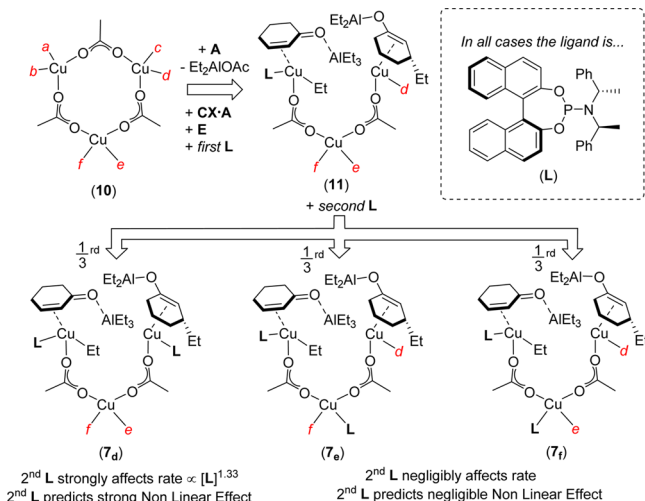| run	$[A]_0$ (mM)	$[CX]_0$ (mM)	$[Cu]_0$ (mM)	$[L]_0$ (mM)	$[CX·A]_0$ (mM)	$[L]_0:[Cu]_0$	k_1 (10^3 s^{-1})[a]
1	0−340	337−406			0−207		
2	0−345	421−481			0−237		
3	520	413	3.46	4.99	300	1.44	1.558(8)
4	402	345	3.18	4.88	232	1.54	1.94(3)
5	255	202	3.55	5.22	124	1.47	0.566(7)
6	125	80.1	3.13	4.76	40.4	1.52	0.240(4)
7	397	337	1.07	1.59	226	1.49	0.323(4)
8	381	327	1.96	3.06	217	1.55	0.490(5)
9	379	321	3.79	5.49	213	1.45	1.517(9)
10	380	311	6.10	8.82	218	1.45	4.33(9)
11	396	351	3.62	1.66	232	0.46	0.674(4)
12	403	397	3.55	3.54	254	1.00	1.066(5)
13	396	339	3.19	6.54	227	2.05	1.94(2)
14	408	332	3.36	11.7	227	3.54	2.76(3)[b]
15	428	362	3.35	13.6	248	4.07	2.60(6)[b]
16	386	330	3.42	15.4	220	4.51	1.63(3)[b]

[a]For consumption of **CX·A**, a value of 1.558(8) equates to $[1.558(8)] \times 10^{-3}$ s^{-1}. [b]First-order fit given to allow direct comparison with other Table 1 data; the zero-order (k_0) rate constants attained for runs 14−16 in Figure 3 are respectively $[4.56(6)] \times 10^{-4}$, $[3.24(3)] \times 10^{-4}$, and $[2.35(2)] \times 10^{-4}$ M s^{-1}.

Scheme 3. Mechanism for Cu I/L 1,4-Addition of AlEt3 (A) to Cyclohex-2-en-1-one (CX) Consistent with All Experimentally Observed Data Herein[a]
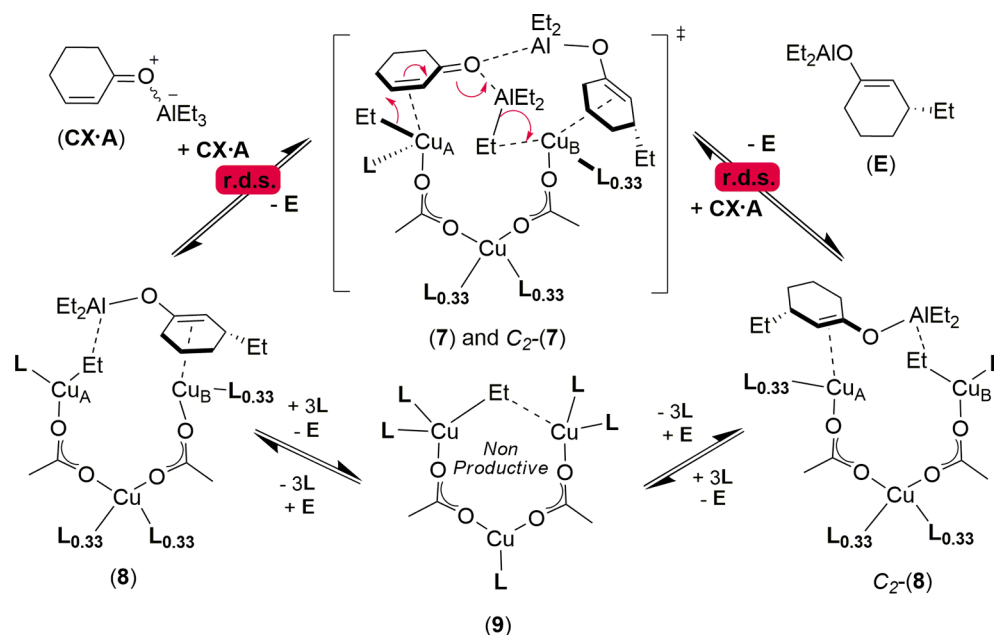
[a]The presence of any metal-coordinated solvent is excluded for clarity; $L_{0.33}$ indicates partial (33%) binding to that site.[22] Each catalytic cycle interconverts Cu_A with Cu_B and their respective roles within the cycle.

period results. In the presence of excess ligand off-cycle inhibition is observed via **9**. Regeneration of **8** from **9** is expected to be zero order in **L** at high [**L**], as observed. We note that the Cu(μ-alkyl)Cu mode proposed for **9** was recently detected crystallographically for a methyl unit.[21] The stoichiometry of **7** $[Cu_3L_2CX_2A_2]$ is in accord with twice the observed rate law $([CX·A]^1[Cu]^{1.5}[L]^{0.66})$, through the

molecularity **E = CX + A**.[22,23] As only the ligand **L** proximal to the catalytic site affects the conjugate addition rate, only this fraction is detected in the kinetic studies; the other Cu**L** units play only a structural role.[22] One explanation for how the Cu_3L_2 unit provides a ligand molecularity of $[L]^{1.33}$ through rapid ligand exchange is shown in Scheme 4. The structure of **8** was confirmed in DFT model studies (**8′** using the ωB97X-D[23]

Scheme 4. Origin of the 1.33 Ligand (L) Molecularity[a]

2nd **L** strongly affects rate ∝ [**L**][1.33]
2nd **L** predicts strong Non Linear Effect

2nd **L** negligibly affects rate
2nd **L** predicts negligible Non Linear Effect

[a]Trigonal $Cu_3(OAc)_3$ (10) has six additional ligand coordination sites (a−f). Loading this with **A**, **CX·A**, **E** and *one* **L** provides structure 11 with three remaining coordination sites (d−f). The *second* **L** loads randomly into these sites. Formation of 7d leads to the "shuttling mechanism" of Scheme 3 and the observed [**L**][1.33] order.

functional and Stuttgart−Bonn pseudopotential and basis set for Cu,[24] with the 6-311G(d) basis set[25] for all other atoms; see the Supporting Information) using a simplified ligand set, which nevertheless indicated the proposed Cu−Et···Al distal contact (C···Al 4.14 Å; see the Supporting Information). The model intermediate **8′** readily coordinated an additional molecule of **CX·A**, and this rapidly evolved toward model species closely related to **7**, in line with the observed molecularity.

The alternative transition state **12** to **7** was also considered (Scheme 5). It is kinetically indistinguishable from **7**, but the

Scheme 5. Discounted Alternative Transition State to 7
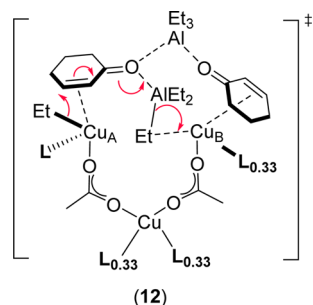
experimental data for the induction period are not consistent with its presence. Our prereduction protocol leads to very rapid catalyst formation from fully homogeneous precursor solutions. While deliberately perturbing these conditions to favor nonhomogeneous systems did result in slower inductions, no product formation was seen in these initial periods. On full dissolution, reaction rates similar to those normally observed operated. This suggests that dissolution effects are not the source of the induction. More importantly, if on completion of the catalytic reaction (Scheme 2, but before quenching) the mixture is redosed with further **CX** and **A**, catalysis restarts immediately, without any induction period and with slightly increased enantioselectivity (3−4% higher than that of the

initial run). This effect is rather supportive of the product **E** being ligated within the selective transition state. While we cannot completely discount **12**, the overall data strongly support **7** being the major contributor.

The presence of a Cu_3L_2 stoichiometry in **7** predicts that the proximal Cu_AL and Cu_BL should lead to diastereomeric transition states if less than 100% ee **L** is used. The proximity of these two ligands in intermediates leading to the rate determination (**7d**) dictates that such a system is expected to show a nonlinear effect (NLE).[26] The enantiopurity of the ligand (**L**) was varied from 0 to 100% ee, and a small positive NLE is experimentally observed when the ee of **L** is below ca. 50% (runs 24−28, Table S1 in the Supporting Information). These experimental data are well simulated by our kinetic model, whereby the homochiral catalyst L_R,L_R provides (*R*)-3-ethylcyclohexanone (**P**) in 82% ee and the heterochiral catalyst L_R,L_S leads to the same enantiomer of product **P** in 99% ee, but this is formed 1.4 times more slowly than the homochiral catalyst (Figures S7 and S8 in the Supporting Information).

■ CONCLUSIONS

Gschwind's hypothesis, that a single dominant copper/phosphoramidite species is responsible for the ACA reactions of "softer" organometallics, is supported by the studies herein. However, our data are most in accord with the major chemical entity responsible for the catalytic 1,4-addition of $AlEt_3$ to cyclohex-2-en-1-one being a Cu_3L_2 trimer rather than the Cu_2L_3 dimer proposed for analogous zinc chemistry. A catalytic cycle involving shuttling between two C_2 symmetry related ground states (**8**) each containing a π-bound enolate and a Cu−Et bond is an attractive proposal, in that (i) it leads to a transition state stoichiometry in line with a simple interpretation of the primary kinetic data, (ii) the −$OAlEt_2$ Lewis acid function of the Cu π-bound enolate offers a favorable additional point of binding and activation for the cyclohex-2-en-1-one/$AlEt_3$ adduct (**CX·A**) as this docks into the catalyst, (iii) the conjugate addition triggers both formation and expulsion of the enolate product (**E**), facilitating fast turnover, (iv) it explains the experimentally observed induction period, (v) it offers a prediction of the observed NLE, (vi) the proposed rds stoichiometry correlates well with older observations that stoichiometric cuprates typically require 2:1 MR:CuX ratios before they become active in additions to enones,[27] and finally (vii) simple DFT computational models are also in accord with the proposal. While the real catalytic mixture undoubtedly contains small populations of other species, the data attained here are most in accord with the major catalytic reaction manifold occurring via the cycle of Scheme 3. The presence of a bound enolate (**E**) within the selective transition state of the 1,4-conjugate addition catalyst is a key finding of this present study. Enolate−catalyst incorporation provides an insight into a long observed but previously unexplained fact: in copper-catalyzed ACA reactions of organoaluminum species the most active and selective catalysts are frequently realized from very labile copper(I) sources, such as $[Cu(MeCN)_4]BF_4$, and it is these species that are of course most predisposed to product enolate incorporation.

■ ASSOCIATED CONTENT

Ⓢ Supporting Information

The Supporting Information is available free of charge on the ACS Publications website at DOI: 10.1021/acscatal.7b02198.

Experimental procedures, derivation of binding isotherms, and primary data for all runs (1−28) and final calculated coordinates for intermediates (*syn-/anti-***CX·A** and models **8′** and **8′-CX·A**) (PDF)

■ AUTHOR INFORMATION

Corresponding Author
*E-mail for S.W.: simon.woodward@nottingham.ac.uk.

ORCID ⓘ
David Robinson: 0000-0003-2760-7163
Simon Woodward: 0000-0001-8539-6232

Notes
The authors declare no competing financial interest.

■ REFERENCES

(1) For general overviews of ACA reactions see: (a) *Copper-Catalyzed Asymmetric Synthesis*; Alexakis, A., Krause, N., Woodward, S., Eds.; Wiley-VCH: Weinheim, Germany, 2014. (b) Thaler, T.; Knochel, P. *Angew. Chem., Int. Ed.* **2009**, *48*, 645−648. (c) Alexakis, A.; Bäckvall, J. E.; Krause, N.; Pàmies, O.; Diéguez, M. *Chem. Rev.* **2008**, *108*, 2796−2823. (d) Falciola, C. A.; Alexakis, A. *Eur. J. Org. Chem.* **2008**, *2008*, 3765−3780. For listings of early developments see: (e) Krause, N.; Hoffmann-Röder, A. *Synthesis* **2001**, *2001*, 0171−0196.

(2) For ligand effects in ACA reactions see: (a) Alexakis, A.; Krause, N.; Woodward, S. Copper-Catalyzed Asymmetric Conjugate Addition. In *Copper-Catalyzed Asymmetric Synthesis*; Alexakis, A., Krause, N., Woodward, S., Eds.; Wiley-VCH: Weinheim, Germany, 2014; pp 33−68 (also covers nucleophile and substrate types). (b) Lopez, F.; Minnaard, A. J.; Feringa, B. L. *Acc. Chem. Res.* **2007**, *40*, 179−188 (phosphoramidites). (c) Harutyunyan, S. R.; den Hartog, T.; Geurts, K.; Minnaard, A. J.; Feringa, B. L. *Chem. Rev.* **2008**, *108*, 2824−2852 (diphosphines, especially Josiphos). (d) Hajra, A.; Yoshikai, N.; Nakamura, E. *Org. Lett.* **2006**, *8*, 4153−4155 (mixed P,O-donors). (e) Germain, N.; Magrez, M.; Kehrli, S.; Mauduit, M.; Alexakis, A. *Eur. J. Org. Chem.* **2012**, *2012*, 5301−5306 (NHC ligands). (f) Palais, L.; Alexakis, A. *Chem. - Eur. J.* **2009**, *15*, 10473−10485 (simplephos)..

(3) For reviews of mechanistic aspects see: (a) Yoshikai, N.; Nakamura, E. *Chem. Rev.* **2012**, *112*, 2339−2372. (b) Woodward, S.; Willcox, D. Ligated Organocuprates: An A-Z Routemap of Mechanism and Application. In *Innovative Catalysis in Organic Synthesis*; Andersson, P. G., Ed.; Wiley-VCH: Weinheim, Germany, 2012; pp 233−255. (c) Jerphagnon, T.; Pizzuti, M. G.; Minnaard, A. J.; Feringa, B. L. *Chem. Soc. Rev.* **2009**, *38*, 1039−1075. (d) Rovis, T.; Evans, D. A. *Prog. Inorg. Chem.* **2002**, *50*, 1−150. (e) Nakamura, E.; Mori, S. *Angew. Chem., Int. Ed.* **2000**, *39*, 3750−3771. (f) Gallo, E.; Ragaini, F.; Bilello, L.; Cenini, S.; Gennari, C.; Piarulli, U. *J. Organomet. Chem.* **2004**, *689*, 2169−2176. (g) Bertz, S. H.; Cope, S.; Murphy, M.; Ogle, C. A.; Taylor, B. J. *J. Am. Chem. Soc.* **2007**, *129*, 7208−7209. For a summary of early work see: (h) Mori, S., Nakamura, E. Mechanisms of Copper-mediated Addition and Substitution Reactions. In *Modern Organocopper Chemistry*; Krause, N., Ed.; Wiley-VCH: Weinheim, Germany, 2002; pp 315−346. (i) den Hartog, T.; Huang, Y.; Fañanás-Mastral,

M.; Meuwese, A.; Rudolph, A.; Pérez, M.; Minnaard, A. J.; Feringa, B. L. *ACS Catal.* **2015**, *5*, 560−574.

(4) For characterized examples of π complexes see: (a) Bertz, S. H.; Hardin, R. A.; Heavey, T. J.; Ogle, C. A. *Angew. Chem., Int. Ed.* **2013**, *52*, 10250−10252 (by X-ray). (b) Uerdingen, M.; Krause, N. *Tetrahedron* **2000**, *56*, 2799−2804 (by ^{13}C NMR). (c) Krause, N.; Wagner, R.; Gerold, A. *J. Am. Chem. Soc.* **1994**, *116*, 381−382 (by ^{13}C NMR).

(5) For copper(III) intermediates (detection method, geometry) see: (a) Chang, H.-C.; Lo, F.-C.; Liu, W.-C.; Lin, T.-H.; Liaw, W.-F.; Kuo, T.-S.; Lee, W.-Z. *Inorg. Chem.* **2015**, *54*, 5527−5533 (X-ray, tbp). (b) Hannigan, S. F.; Lum, J. S.; Bacon, J. W.; Moore, C.; Golen, J. A.; Rheingold, A. L.; Doerrer, L. H. *Organometallics* **2013**, *32*, 3429−3436 (X-ray, square planar). (c) Bertz, S. H.; Hardin, R. A.; Murphy, M. D.; Ogle, C. A.; Richter, J. D.; Thomas, A. A. *J. Am. Chem. Soc.* **2012**, *134*, 9557−9560 (NMR, trigonal π-allyl). (d) Casitas, A.; King, A. E.; Parella, T.; Costas, M.; Stahl, S. S.; Ribas, X. *Chem. Sci.* **2010**, *1*, 326−330 (X-ray, square based pyramidal). (e) Bartholomew, E. R.; Bertz, S. H.; Cope, S. K.; Murphy, M. D.; Ogle, C. A.; Thomas, A. A. *Chem. Commun.* **2010**, *46*, 1253−1254 (NMR, square planar). (f) Bertz, S. H.; Murphy, M. D.; Ogle, C. A.; Thomas, A. A. *Chem. Commun.* **2010**, *46*, 1255−1256 (NMR, square planar). (g) Bartholomew, E. R.; Bertz, S. H.; Cope, S.; Dorton, D. C.; Murphy, M.; Ogle, C. A. *Chem. Commun.* **2008**, 1176−1177 (NMR, square planar, ligated). (h) Bertz, S. H.; Cope, S.; Murphy, M.; Ogle, C. A.; Taylor, B. J. *J. Am. Chem. Soc.* **2007**, *129*, 7208−7209 (NMR, square planar). For an introductory overview of this area see: (i) Bertz, S. H.; Cope, S.; Dorton, D.; Murphy, M.; Ogle, C. A. *Angew. Chem., Int. Ed.* **2007**, *46*, 7082−7085.

(6) Harutyunyan, S. R.; López, F.; Browne, W. R.; Correa, A.; Peña, D.; Badorrey, R.; Meetsma, A.; Minnaard, A. J.; Feringa, B. L. *J. Am. Chem. Soc.* **2006**, *128*, 9103−9118.

(7) Pfretzschner, T.; Kleemann, L.; Janza, B.; Harms, K.; Schrader, T. *Chem. - Eur. J.* **2004**, *10*, 6048−6057.

(8) Kitamura, M.; Miki, T.; Nakano, K.; Noyori, R. *Bull. Chem. Soc. Jpn.* **2000**, *73*, 999−1014. These workers attributed their induction period to catalyst dissolution effects.

(9) (a) Zhang, H.; Gschwind, R. M. *Angew. Chem., Int. Ed.* **2006**, *45*, 6391−6394. (b) Zhang, H.; Gschwind, R. M. *Chem. - Eur. J.* **2007**, *13*, 6691−6700. (c) Schober, K.; Zhang, H.; Gschwind, R. M. *J. Am. Chem. Soc.* **2008**, *130*, 12310−12317. (d) von Rekowski, F.; Koch, C.; Gschwind, R. M. *J. Am. Chem. Soc.* **2014**, *136*, 11389−11395. For an overview of NMR applications in cuprate catalysis see: (e) von Rekowski, F.; Koch, C.; Gschwind, R. M. NMR Spectroscopic Aspects. In *Copper-Catalyzed Asymmetric Synthesis*; Alexakis, A., Krause, N., Woodward, S., Eds.; Wiley-VCH: Weinheim, Germany, 2014; pp 353−372. (f) Gschwind, R. M. *Chem. Rev.* **2008**, *108*, 3029−3053.

(10) Pàmies, O., Diéguez, M. Conjugate Addition of Organo-aluminum Species to Michael Acceptors and Related Processes. In *Modern Organoaluminum Reagents*; Woodward, S., Dagorne, S., Eds.; Springer: New York, 2013; pp 277−306.

(11) Other options for catalytic asymmetric additions of alkyl nucleophiles to β,β-substituted enones exist, notably zirconium reagents. For recent examples see: (a) Gao, Z.; Fletcher, S. P. *Chem. Science* **2017**, *8*, 641−646. (b) Garrec, K.; Fletcher, S. P. *Org. Lett.* **2016**, *18*, 3814−3817.

(12) The only rate study we can identify is an early qualitative correlation of [Cu] to initial rate for a ligandless system: Kabbara, J.; Flemming, S.; Nickisch, K.; Neh, H.; Westermann, J. *Chem. Ber.* **1994**, *127*, 1489−1493.

(13) The only related measurement we could identify was AlMe(2,6-tBu$_2$-4-MeC$_6$H$_2$O)$_2$ with benzophenone in toluene-d_8: K(35 °C) = 38.2 M^{-1}, ΔH_f° = 67.1 kJ mol^{-1} (16.0 kcal mol^{-1}): (a) Power, M. B.; Nash, J. R.; Healy, M. D.; Barron, A. R. *Organometallics* **1992**, *11*, 1830−1840. A ketone complex of AlEtCl$_2$ has been identified by ^{1}H NMR spectroscopy but no binding (association) constant was measured: (b) Childs, R. F.; Duffey, B. M.; Mahendran, M. *Can. J. Chem.* **1986**, *64*, 1220−1223.

(14) The presence of such R_3Al−enone adducts has been widely assumed to be the reason for the enhanced activity of alanes in the formation of quaternary centers in ACA reactions, but they had remained undetected. See: Alexakis, A.; Krause, N.; Woodward, S. Copper-Catalyzed Asymmetric Conjugate Addition. In *Copper-Catalyzed Asymmetric Synthesis*; Alexakis, A., Krause, N., Woodward, S., Eds.; Wiley-VCH: Weinheim, Germany, 2014; pp 33−68),.

(15) Reduction is rapid and complete under such conditions. See: (a) Yan, M.; Yang, L. W.; Wong, K. Y.; Chan, A. S. C. *Chem. Commun.* **1999**, 11−12 (NMR study). (b) Pfretzschner, T.; Kleemann, L.; Janza, B.; Harms, K.; Schrader, T. *Chem. - Eur. J.* **2004**, *10*, 6048−6057 (EPR study). Reduction to Cu^I before catalysis also avoids the potential for competing radical effects. See: (c) Li, K.; Alexakis, A. *Angew. Chem., Int. Ed.* **2006**, *45*, 7600−7603.

(16) In fact, in favorable examples these may be isolated: Mothes, R.; Ruffer, T.; Shen, Y.; Jakob, A.; Walfort, B.; Petzold, H.; Schulz, S. E.; Ecke, R.; Gessner, T.; Lang, H. *Dalton Trans.* **2010**, *39*, 11235−11247.

(17) For the technique used see: Canisius, J.; Gerold, A.; Krause, N. *Angew. Chem., Int. Ed.* **1999**, *38*, 1644−1646.

(18) The greater data density of the ReactIR studies allowed us to confidently discriminate between various empirical rate laws. Consistently better fits were attained for the first-order disappearance of **CX·A** (vs zero order, second order, and first order near equal concentration) rate laws on the basis of R^2 values. Consistent with this picture, a switch to zero-order behavior at high **L** concentrations was detected. For lower data dentist GC data points were fitted only to first-order behavior. See also the Supporting Information.

(19) Blackmond, D. G. *Angew. Chem., Int. Ed.* **2005**, *44*, 4302−4320.

(20) Alexakis, A.; Benhaim, C. *Eur. J. Org. Chem.* **2002**, *2002*, 3221−3236.

(21) Molteni, R.; Bertermann, R.; Edkins, K.; Steffen, A. *Chem. Commun.* **2016**, *52*, 5019−5022.

(22) An alternative model where each of the four coordination sites on the three coppers has an occupancy of one-third was also considered. This is mechanistically indistinguishable from Schemes 3 and 4. Phosphorus-31 NMR studies under reaction conditions identical with those of the kinetic studies show only a single ^{31}P signal (144.5 ppm), confirming ligand exchange. All such valid structures for **7** have the stoichiometry $Cu_3L_2CX·A·E$, equivalent to $Cu_3L_2CX_2A_2$ through the molecularity $E = CX + A$.

(23) Chai, J.-D.; Head-Gordon, M. *Phys. Chem. Chem. Phys.* **2008**, *10*, 6615−6620.

(24) Dolg, M.; Wedig, U.; Stoll, H.; Preuss, H. *J. Chem. Phys.* **1987**, *86*, 866−872.

(25) Krishnan, R.; Binkley, J. S.; Seeger, R.; Pople, J. A. *J. Chem. Phys.* **1980**, *72*, 650−654.

(26) Girard, C.; Kagan, H. B. *Angew. Chem., Int. Ed.* **1998**, *37*, 2922−2959.

(27) Alexakis, A.; Benhaim, C.; Rosset, S.; Humam, M. *J. Am. Chem. Soc.* **2002**, *124*, 5262−5263.